BLADE PLANFORM OPTIMIZATION FOR A DUAL SPEED ROTOR CONCEPT

Antonio Visingardi, a.visingardi@cira.it, CIRA (Italy)
Luigi Federico, l.federico@cira.it, CIRA (Italy)
Mattia Barbarino, m.barbarino@cira.it, CIRA (Italy)

Abstract

The paper illustrates the results of a multi-objective optimization activity performed on the blade planform shape of a medium-size helicopter in order to maximize the beneficial effects of a dual speed rotor technology and to provide a new baseline configuration for the possible application of active devices for the further improvements of the rotor performance. The optimization is performed with the aim to minimize the average total power and the average OASPL for four different flight conditions: a cruise flight and a max-speed level flight at full rotor speed and a 14.3° climb and a 6° descent flight at 90%RPM rotor speed. Additional flight conditions are tested after the optimization in order to further verify the benefits of the optimization. The planform shape is optimized by modifying the sectional chord lengths, the local sweep angles and the local twist angles of selected design points within given constraints. The commercial aeromechanics code FlightLab and the in-house aeroacoustic module OptydB_FRN have been selected as the best compromise between accuracy of the results and moderate CPU requirements. These tools, along with a planform modeller, are arranged in an optimization workflow that was built by using the commercial simulation framework toolkit Optimus® by Noesis. A genetic algorithm is used for the optimization phase. The built-up optimization procedure and the application of the described computational tools, with their respective peculiarities, advantages and limitations, demonstrate to be effective at producing reasonable performance improvements. The combined effects of rotor speed reduction and planform optimization produce power reductions ranging from 3.52%, in hover flight, to 5.96%, in fly-over flight, and noise reductions ranging from 1.88dB, in fly-over flight, to 3.40dB, in descent flight.

1 NOMENCLATURE

A	acoustic hemisphere surface area
bpf	blade passage frequency
c	chord length
C_T/σ	blade loading
C_W	weight coefficient
D	section drag coefficient
L	section lift coefficient
p	acoustic pressure
p_{ref}	reference pressure
$\overline{P}$	time-averaged total power
R	rotor radius
$\overline{SPL}$	time-averaged overall sound pressure level
μ	rotor advance ratio
σ	rotor solidity

2 INTRODUCTION

The improvement of a helicopter performance is a vital aspect of the rotorcraft operation on which a constant effort is being made by the international helicopter community. The complexity of rotorcraft aeromechanics and the large range of operations of the rotor blade often demand the simultaneous fulfilment of conflicting requirements and therefore make the improvement of performance an extremely challenging area in rotorcraft research and design.

The possibility of varying the rotor speed is one means of improving the performance of a helicopter since it allows as many blade elements as possible to operate at or near the angle of attack of maximum lift-to-drag ratio at different flight conditions[1].

A widely variable speed rotor is the technology that exploits at the best the advantage of a rotor speed variation but can show the disadvantage to introduce high rotor vibrations in a wide range of frequencies that are excited due to the different rotor speeds. These vibrations are transmitted to the fuselage which must be therefore carefully designed to avoid multiple resonances.

The dual speed rotor (DSR) concept offers the possibility to operate the rotor at two speeds only, thus representing a simplification of the variable speed rotor, but shows the main advantage to be realized through an engine speed control, thus avoiding the installation of complex and heavy transmissions requiring additional power to be operated. It also limits the rise of resonance phenomena on the fuselage.

Both the dual and the widely variable speed rotor technologies can operate stand-alone or in combination with other technologies to further improve the performance of a helicopter[2].

Tilt-rotor aircraft (e.g. V-22 and AW609), compound helicopters (e.g. Lockheed AH-56), co-axial helicopters (e.g. Sikorsky S-97 Raider) are examples of configurations where some degree of rotor speed reduction is applied for high cruise speeds. The Bell 407 helicopter reduces the rotor speed during cruise to limit fly-over noise while the Sikorsky S-76D operates the rotor in high- and low-speed modes for improved takeoff, hover and cruise performance and reduced noise. Other helicopters reduce the speed

during takeoff and landing for noise limitations. An example of a widely variable speed rotor is instead represented by Boeing's recent A160T Hummingbird.

2.1 Dual Speed Rotor technology

In the framework of the European research programme CleanSky JTI – Green Rotorcraft (GRC) ITD[3], the study of a DSR was promoted for the power reduction and noise abatement of a medium-size helicopter rotor. The DSR must operate at both the nominal speed (100%RPM) and a reduced speed that project specifications have fixed to 90%RPM.

This paper illustrates a multi-objective procedure that has been set up in the framework of the JTI-GRC project for the blade planform optimization of a medium-size helicopter rotor in order to exploit in a more efficient way the DSR concept for the performance improvement.

The structure of the paper is as follows: sections 3 and 4 illustrate respectively the baseline rotor characteristics and the flight conditions selected for the optimization activity. The design and optimization procedures are described in sections 5 and 6. The computational tools employed in the present investigation are briefly illustrated in section 7. The outcomes of the optimization are described in section 8 whereas the results of the performance improvement are illustrated in section 9. Some conclusions are finally provided in section 10.

3 THE BASELINE ROTOR

The baseline configuration is a four-bladed rotor. The blade planform is rectangular up to the 95% of the span and followed by a tip with parabolic leading edge, Figure 1.

The radius R of the blade is 8.15 m and the main chord length c is equal to 0.65 m. A NACA23012 airfoil spans from the blade root cut-out to the 75% of the radius; an OA209 airfoil is mounted from 90% of the span to the tip, whereas a linear interpolation between these two airfoils provides the airfoil geometry in the range between the 75% to the 90% of the blade span. The nominal rotor speed is equal to 250.74 RPM.

4 FLIGHT CONDITIONS

Four flight conditions were selected for running the blade planform optimization procedure. They are highlighted in red in Table 1 and consist in:

- Cruise flight – 80 kts @ 100% RPM;
- Max-speed level flight – 160 kts @100 RPM;
- 14.3° Climb flight – 80 kts @ 90% RPM;
- 6° Descent flight – 80 kts @ 90% RPM.

FLIGHT CONDITION	SPEED (Knots)	ROTOR SPEED	ADVANCE RATIO	CT/σ	CW
Cruise	80	100%	0,19	0,12	0,0128
Max speed	160	100%	0,38	0,08	0,0086
Flyover	120	100%	0,29	0,08	0,0086
Flyover	120	90%	0,32	0,10	0,0106
14,3° Climb	80	100%	0,19	0,08	0,0086
14,3° Climb	80	90%	0,21	0,10	0,0106
6° Descent	80	100%	0,19	0,10	0,0107
6° Descent	80	90%	0,21	0,13	0,0132
HOGE	0	100%	0,00	0,10	0,0107
HOGE	0	90%	0,00	0,13	0,0132

Table 1: Flight conditions

The resulting improvement in the performance of the optimized rotor was further verified by performing post-optimization calculations for the whole set of the flight conditions indicated in Table 1.

5 DESIGN PROCEDURE

The design procedure consisted in the optimization of the blade planform by varying, within given ranges and according to defined constraints, the main parameters affecting the blade planform in order to achieve specific objectives.

5.1 Parameters

Three geometric parameters were identified for the blade planform modification:

- sectional chord;
- local sweep angle;
- local twist angle.

Five radial stations were selected as design points: 20%; 40%, 75%, 95% and 100%.

The baseline airfoil sections NACA23012 and OA209 were kept unchanged.

5.2 Constraints

The specifications set in the JTI-GRC project imposed some constraints for the sectional chord lengths, the maximum quarter-chord sweep angle, and the total twist angle of the blade, Table 2. In particular, the chord was indicated to vary within a range of [0.8; 1.3] times the nominal chord length all along the blade radius up to the radial section at 95%. In the remaining 5% the minimal chord length was tolerated to be equal to 40% of the nominal chord. The maximum quarter-chord sweep angle was indicated not to exceed 45°, whereas a higher value was allowed at the blade tip. The total twist was specified to vary within 6° and 18°.

r/R	Unit	47%	75%	95%	100%
Nominal chord	m	0,6500	0,6500	0,6500	0,2168
Min chord ratio		0,8000	0,8000	0,8000	0,4000
Min Chord	m	0,5200	0,5200	0,5200	0,0867
Max chord ratio		1,3000	1,3000	1,3000	1,3000
Max Chord	m	0,8450	0,8450	0,8450	0,2818
Max Sweep	deg	45	45	45	> 45
Twist Range	deg	6 to 18	6 to 18	6 to 18	6 to 18

Table 2: Assigned constraints

On the basis of the assigned constraints, those that were effectively applied were inferred by considerations of technical feasibility:

- the blade should be kept as much as possible unaltered in the first 50% of the span in order not to degrade its main structural properties;
- an increase in chord length in the outboard region of the blade would increase the profile power thus hampering the total power reduction;
- highly swept blades would promote the rise of aeroelastic instabilities.

Table 3 illustrates, with coloured figures, the nine applied constraints, three for each selected parameter, and their range of variability.

	r/R	0,20	0,47	0,75	0,95	1,00
Chord (m)	Low	0,6500	0,6500	0,5800	0,5800	0,0867
	Nominal	0,6500	0,6500	0,6500	0,6500	0,2168
	High	0,6500	0,6500	0,6500	0,6500	0,2168
C/4 Sweep angle (deg)	Low	0,0000	-2,0000	0,0000	25,0000	
	Nominal	0,0000	0,0000	0,0000	46,7500	
	High	0,0000	3,0000	5,0000	46,7500	
Twist (deg)	Low	4,4010	1,6390	-5,0000	-5,0000	-5,0000
	Nominal	4,4010	1,6390	-1,0990	-1,3940	-1,9270
	High	4,4010	1,6390	0,0000	0,0000	0,0000

Table 3: Applied constraints

In particular, the chord was only allowed to reduce its length and a small negative sweep was allowed at 47% of the blade radius only.

5.3 Objectives

For each of the four flight conditions selected the rotor time-averaged total power $\overline{P}$ and the averaged sound pressure level $\overline{SPL}$ were evaluated. The power averaging was performed over one rotor revolution in trimmed conditions, whereas the averaged OASPL was obtained by averaging the acoustic pressures evaluated on the surface of a hemisphere, described in section 9.2, according to the following equation:

(1) $$\overline{SPL} = 20\ Log\left(\frac{\frac{1}{A}\int p\,dA}{p_{ref}}\right)$$

The design objectives were identified in the minimization of two global objective functions, OBJ_1 and OBJ_2 respectively defined as the two following weighted averages:

(2) $$OBJ_1 = \pi_1\overline{P_1} + \pi_2\overline{P_2} + \pi_3\overline{P_3} + \pi_4\overline{P_4}$$

(3) $$OBJ_2 = \nu_1\overline{SPL_1} + \nu_2\overline{SPL_2} + \nu_3\overline{SPL_3} + \nu_4\overline{SPL_4}$$

In order to set suitable weights in the two objective functions, a preliminary computation of the total power $\overline{P}$ and the $\overline{SPL}$ was performed for the four flight conditions in full rotor speed conditions. With reference to the power, the figures illustrated in Table 4 indicated that:

1. the descent flight requires less than half the power of the other flight conditions, thus not representing a real objective to be minimized;
2. climb, which requires the highest power, is usually a flight conditions in which the helicopter operates for a shorter time with respect to cruise and/or max speed flight.

For these reasons, the weights π_i were assigned the following values: $\pi_1 = 0.30$; $\pi_2 = 0.40$; $\pi_3 = 0.00$; $\pi_4 = 0.30$.

Concerning the noise, the reduction in $\overline{SPL}$ during cruise and max speed was deemed of little importance since these two flight conditions are performed at high altitudes, thus not causing much discomfort to the community. For this reason, the weights ν_i were assigned the following values: $\nu_1 = 0.00$; $\nu_2 = 0.00$; $\nu_3 = 0.50$; $\nu_4 = 0.50$.

	Flight conditions @ 100%RPM	$\overline{P}$ (HP)	$\overline{SPL}$ (dB)
1	Cruise	1688	90,16
2	Max Speed Level	1792	94,83
3	6° Descent	824	93,87
4	14.3° Climb	2001	83,88

Table 4: Baseline rotor - Total Power and Noise vs Flight conditions

6 OPTIMIZATION PROCEDURE

A multi-objective procedure was applied for the blade planform optimization and the commercial simulation framework toolkit Optimus®, revision 10, by Noesis[4], was used for this purpose. The workflow and the optimization algorithm are described in the following.

6.1 Workflow

The workflow built for the optimization procedure is illustrated in Figure 2 and consists of three main modules:

- Input module;
- Action module;
- Output post-processing module.

In the input module, all the design parameters are specified with the relative constraints. The action module consists of three computational tools: a blade planform modeller, an aeromechanic solver and an aeroacoustic solver. Since the planform optimization is performed over two couples of flight conditions, two branches depart from the planform modeller. The workflow shows on the upper side the branch relative to the flight conditions at 100% RPM and on the lower side the branch relative to the flight conditions at 90%RPM. The branches are perfectly symmetrical. The output module deals with the extraction and post-processing of the output variables for the two couples of flight conditions as well as their linear combination for the evaluation of the above described global objective functions. Additionally, two control outputs, “TW chord” and “Failure”, are respectively produced for monitoring the thrust-weighted chord (a measure of the solidity); and the occurrence of untrimmed flight conditions (which are then discarded).

6.2 Optimization algorithm

The multi-objective non-dominated sorting genetic algorithm NSEA+ was used. A number of 12 iterations was performed on a population size of 20 individuals for the detection of the optimal solutions (Pareto front), thus summing up to a total number of 240 experiments.

7 COMPUTATIONAL TOOLS

7.1 Planform modeller

The planform modeller was an in-house tool developed for the creation of the blade geometry once assigned the sectional chord length, the quarter chord line position and the twist angle in the five radial stations specified in section 5.2. The radial stations determine four blade patches for each of which piece-wise quadratic splines describe the chord and the quarter chord line position, while a piece-wise linear interpolation describes the blade twist law.

7.2 Aeromechanic solver

The commercial code FlightLab[5],[6],[7], which is widely applied for rotorcraft aeromechanic modelling, was used for the evaluation of the aerodynamic characteristics of both the baseline and the optimized rotors. The choice of such a comprehensive tool was motivated by the necessity to provide in a reasonable CPU time sufficiently accurate aeromechanic results for a large number of experiments required by the optimization procedure.

The rotor aerodynamic model employs 2D look-up tables and includes a 2D indicial formulation to account for unsteady blade sectional airloads.

The rotor induced flow dynamics was evaluated by using two different wake models: the finite state wake model[8],[9], with 45 state variables producing 8 inflow harmonics, was used for all the flight conditions except for the descent flight; a more sophisticated and CPU demanding free-wake model[10] adapted from Leishman's free-wake algorithm[11],[12] was instead applied in order to capture, the higher frequency interactional phenomenologies occurring during descent flight.

A structural dynamic module consisting of a non-linear flexible beam element model for the blade elasticity including a linear lag damper and a pitch-link control was applied.

7.2.1 Validation of the aeromechanic model

Preliminary power estimations were made with FlightLab using a finite-state wake model in order to evaluate the level of fidelity obtainable by the selected aeromechanic modelling. Numerical predictions were made by using the FlightLab-embedded UH-60A helicopter model and the results were compared with the flight test measurements produced during the campaign of the NASA/Army UH-60A Airloads programme[13], [14].

Figure 3 illustrates the power estimations at various advance ratios for four weight coefficients. The agreement with the experiment is very satisfactory for the lower weight coefficients from $C_W = 0.0074$ to $C_W = 0.0091$. A progressive underestimation at advance ratios higher than $\mu = 0.20$ can instead be observed for the higher weight coefficient $C_W = 0.010$. Since the optimization does not alter the helicopter weight and the flight conditions, these differences are expected to remain more or less the same for both the baseline and the optimized rotors thus providing, at the worst, and underestimated power in absolute terms, but no effect on the evaluation of the power reduction.

7.3 Acoustic solver

The in-house aeroacoustic code OptydB_fwh[15],[16], based on Farassat's formulation 1A of the Ffowcs Williams-Hawkings equation, was used for the noise evaluation.

In order to use compact sources data provided by the aeromechanic code, the Fast Rotor Noise (FRN)[16] model was used in combination with OptydB_fwh. This approach allowed a significant reduction of the computational time, while preserving an acceptable level of accuracy.

The FRN model is based on the classical idea of replacing the rotor blade by an equivalent distribution of chordwise compact sources. Under the hypothesis of far-field and geometric compactness conditions, the chordwise pressure distribution, Figure 4a, can be approximated by a compact dipole through an equivalent constant pressure distribution that provides the same aerodynamic loads, Figure 4b

Moreover, in order to model the effect of the flow displacement due to the blade motion (thickness noise), an equivalent monopole is introduced by considering a blade section of equivalent area. The blade is therefore modelled as a spanwise sequence of wedges that undergo the same motion of the original blade, Figure 5.

7.3.1 Validation of the FRN module

Preliminary acoustic analyses were performed in order to assess the level of approximation with which the FRN is able to evaluate a noise carpet. Three experimental test cases investigated in the European project HeliNOVI[17] were evaluated and compared with the corresponding experimental ones. Despite the HeliNOVI model consisted in a full helicopter configuration, the computations were limited to the isolated main rotor. The blade geometry, the kinematics and the load distributions along the blade span were evaluated by FlightLab using a free-wake model and used to feed the FRN model. An acceptable prediction in terms of the noise directivity pattern was observed for all the examined flight conditions. The noise levels were predicted with an error of about 3dB, which is acceptable in consideration of the low level of sophistication of the numerical tools. Figure 6 illustrates an example of the numerical-experimental noise carpets, in a range of frequencies 6^{th} to 40^{th} bpf, obtained for a 6° descent flight. As for the power estimations, also in this case the quantitative differences are expected not to have a great effect on the evaluation of the gain in noise reduction that the blade optimization can produce.

8 OPTIMIZATION RESULTS

Figure 7 illustrates the results of the multi-objective optimization procedure applied. Starting from the baseline planform (red square), 240 experiments (black bullets) were performed by the genetic algorithm in order to produce the Pareto front indicated in the picture with blue line and squares. With respect to the baseline solution, the candidate solutions lying on the front show a reduction in

the time-averaged power - objective function OBJ_1 - of about 10 to 60HP, and an average reduction of about 1.5dB in the $\overline{SPL}$ – objective function OBJ_2 - with a small degree of variability. Therefore, the Pareto front results to be quite flat in the direction of OBJ_2 and for this reason the choice of the optimal planform was made by selecting the one of the Pareto front requiring the lowest power.

An interesting outcome of the optimization concerned the evolution of the design objectives for the descent flight during the optimization. As indicated in Figure 8, unlike the other flight conditions, a reduction in the $\overline{SPL}$ was obtained in descent flight only at the expense of an increase in the total power. Therefore the choice of the optimal solution was in this case a real trade off between the two objective functions.

The evolution of the design parameters during the optimization procedure is shown in Figure 9. As the optimization goes on all the chord lengths ranging between the assigned constraints are investigated, Figure 9a. The experiments falling on the Pareto front show the tendency of the optimization to minimize the chord length. This behaviour finds an explanation in the reduction in profile power that a reduced chord length implies, thus providing a net reduction in total power. The evolution of the sweep angles, Figure 9b, shows the clear tendency of the optimization to redistribute the high sweep of the baseline blade, concentrated in the tip region, to a wider blade span but with lower local values. The justification of this result can be found in two counteracting effects that the sweep has on the rotor performance: on the one hand, sweeping the leading edge of the blade reduces the local Mach number normal to the leading edge of the blade, thus reducing the rise of compressibility effects that produce an increase in the required rotor power; on the other, the amount of sweep must be kept low enough so that there are no inertial couplings introduced into the blade dynamics by an aft centre of gravity or by aerodynamic couplings produced by a rearward centre of pressure[18] that introduce structural overloads. Figure 9c illustrates the evolution of the blade twist. The genetic algorithm investigates all possibilities in the given ranges set by the assigned constraints. However, the experiments lying on the Pareto front show the tendency of the optimization to increase the geometric negative pitch. This result is explained by taking in mind the effect that a reduced chord length has on the rotor thrust. Indeed, since the rotor thrust must be kept constant, a reduced chord length requires an increase in the blade collective pitch. As a consequence, some airfoil sections along the blade, especially toward the tip, may reach effective angles of attack close to or beyond stall conditions thus producing an increase in profile drag. A more negative twist has therefore a beneficial effect in delaying or avoiding this event.

The blade chord, sweep and twist distributions resulting from the optimization are illustrated in Figure 10 and compared with those of the baseline blade. The planform shape of the baseline and optimized blades are shown in Figure 11. In comparison with the baseline blade, the optimized blade is characterized by a 7% reduced thrust-weighted average chord resulting in a consequent reduced solidity and increase in blade loading.

9 PERFORMANCE IMPROVEMENT

Table 5 and Table 6 summarize the rotor performance improvements, expressed in terms of total power and noise reductions, obtained from the optimization of the blade planform for all the ten flight conditions considered. Cruise flight and max-speed level flight have been analysed only at full rotor speed, being this a specific requirement of the JTI-GRC project, whereas the remaining flight conditions have been analysed at both full rotor speed and 90%RPM.

9.1 Total Power reduction

POWER	Cruise	Max Speed	Flyover	Climb	Descent	Hover
Baseline 100%RPM	1688	1792	1150	2001	824	2386
Baseline 90%RPM			1103	1944	802	2352
Delta % - Baseline			4,10	2,86	2,60	1,43
Optimal 100%RPM	1616	1728	1119	1959	837	2332
Optimal 90%RPM			1082	1914	843	2302
Delta % - Optimal			3,30	2,30	-0,70	1,27
Delta % - Bsl.-Opt. 100%	4,29	3,56	2,76	2,09	-1,63	2,28
Delta % - Bsl.-Opt. 90%			1,94	1,53	-5,08	2,13
Delta % - Total	4,29	3,56	5,96	4,34	-2,35	3,52

Table 5: Total Power reduction

From the analysis of Table 5 the following considerations can be made:

1. the rotor speed reduction generally produces a lower requirement of total power since the compressibility phenomena and the total drag are reduced;
2. the optimized blade planform is more effective at reducing the total power at both full and 90%RPM since the airfoil sections are able to work in a more efficient way;
3. the combined effect of rotor speed reduction and planform optimization produces a performance degradation in descent flight;
4. the dual speed rotor technology applied to the optimized rotor is able to provide a reduction in total power ranging from 64 HP in max-speed level flight at 100%RPM to 87 HP in climb flight at 90%RPM. In percentage terms, performance improvements ranging form 3.52% to 5.96% are obtained. The maximum power reduction is obtained in fly-over level flight at 90%RPM.

A more in-deep explanation of how the planform optimization helps reducing the rotor total power can be obtained by analysing Figure 12 which refers, just as an example, to the fly-over level flight. The plotted diagrams show the effective angles of attack at various sections of both the baseline blade at full rotor speed and the optimized blade at 90%RPM rotor speed as a function of the effective Mach number. These diagrams also show a set of curves obtained from the look-up tables employed for the aeromechanic analysis and representing the angles of attack corresponding to the maximum $L^{3/2}/D$ and L/D ratios as well as the L_{MAX} curve and the upper and lower boundaries of the drag bucket of the airfoils employed along the blade. The closer the effective angles of attack are to the maximum $L^{3/2}/D$ and inside the drag bucket the lower is the profile power. Indeed, by comparing the results obtained for the baseline blade with those of the optimized blade this is what can be observed

with particular emphasis for the blended airfoil and the OA209 airfoil sections. Furthermore, this comparison also shows how the reduced rotor speed is able to avoid the overcoming of the drag divergence Mach number, represented by the red vertical line, in the outboard region of the blade, thus reducing the occurrence of compressibility phenomena and contributing to the reduction of the total power required by the rotor.

9.2 Noise reduction

The combined effects of the blade planform optimization and the rotor speed reduction to 90% RPM on the reduction of rotor noise was evaluated by computing the $\overline{SPL}$ on the surface of a hemisphere centred in the rotor hub and having radius of 150m and azimuth and polar discretizations of 20°, Figure 13a. The results are summarized in the following Table 6.

NOISE	Cruise	Max Speed	Flyover	Climb	Descent	Hover
Baseline100%RPM	90,16	94,83	88,47	83,88	93,87	80,63
Baseline 90%RPM			86,06	81,81	92,36	78,00
Gain dB - Baseline			2,41	2,08	1,51	2,63
Optimal 100%RPM	90,17	92,70	89,29	83,31	93,20	79,67
Optimal 90%RPM			86,59	81,29	90,47	77,40
Gain dB - Optimal			2,70	2,02	2,73	2,27
Gain dB - Bsl.-Opt. 100%	-0,01	2,13	-0,81	0,57	0,67	0,96
Gain dB - Bsl.-Opt. 90%			-0,53	0,52	1,89	0,60
Gain dB - Total	-0,01	2,13	1,88	2,59	3,40	3,23

Table 6: Noise reduction

From the analysis of these data the following considerations can be made:

1. in accordance with the outcomes of other investigations[19], the results confirm the rotor speed reduction as the most efficient means for reducing the rotor noise. These reductions have been higher than 2dB;
2. hover is the flight condition of the baseline rotor which receives the highest benefit from the rotor speed reduction. This is produced only by the attenuation of the low-frequency sound pressure levels since the high unsteadiness of the interactional phenomena, which are responsible for the high-frequency sound pressure levels, are negligible during this flight condition;
3. instead, the descent flight has considerably benefited from the blade planform optimization which has produced an attenuation of the interactional phenomena. Indeed, the noise reduction has been increased from the 1.51dB for the baseline rotor to 2.73dB for the optimized rotor;
4. despite the max-speed flight has not been considered as a significant flight condition for the noise reduction, a benefit of 2.13dB has been obtained from the optimization. In consideration of the fact that this flight condition has been evaluated only at full rotor speed conditions, this result can be interpreted as the direct consequence of remodelling the sweep angle distribution along the blade;
5. the dual speed technology applied to the optimized rotor is able to produce global noise reductions ranging from 1.88dB for the fly-over flight to 3.40dB for the descent flight that has confirmed to be the flight condition more positively impacted by the blade planform optimization;
6. no benefits have been observed for cruise flight.

Figure 13b to Figure 13d illustrate an example of the combined effects that the rotor speed reduction and the blade planform optimization produce on the noise contour maps, expressed in terms of SPL, for descent flight. The maps show the progressive noise reduction that is obtained passing from the baseline rotor at full rotor speed, Figure 13b, to the baseline rotor at reduced rotor speed, Figure 13c, to the final optimized rotor at reduced rotor speed. The total noise reduction, evaluated on the max OASPL is equal to 3.40dB.

A more phenomenological interpretation of the noise reduction in descent flight produced by the planform optimization is provided in Figure 14. This figure shows an example of a noise spectrum, evaluated in the region of the hemisphere subject to the highest noise, as a function of the blade passage frequencies (bpf) where each bpf, for the analysed baseline rotor, is about equal to 16.7Hz. The rotor speed reduction produces two main effects: a shift toward lower frequencies, and an attenuation of the noise peaks. The attenuation in the first two bpf, from 0 to about 34Hz, can be explained only by the rotor speed reduction. At higher bpf, from 11 onward, the attenuation that is produced by the rotor speed reduction becomes more evident when passing from the baseline rotor to the optimized rotor, a clear indication that the planform optimization has been able to reduce the interactional phenomena between the blade and the wake and/or the tip vortex.

10 CONCLUSIONS

The aim of this paper was to illustrate the results of a multi-objective optimization activity performed on the blade planform shape of a medium-size helicopter rotor in order to:

- maximize the beneficial effects of a dual speed rotor technology promoted in the framework of the European research project JTI Green Rotorcraft “Innovative Rotor Blade”;
- provide a new baseline configuration for the possible application of active devices for further improvements of the rotor performance.

The built-up optimization procedure and the application of the described computational tools, with their respective peculiarities, advantages and limitations, demonstrated to be effective at producing reasonable performance improvements not only for the flight conditions selected for the optimization but also for the other flight conditions tested for the post-optimization verification purposes.

From the analysis of the results obtained the following conclusions may be drawn:

1. with respect to the baseline blade, the optimized planform shape is characterised by smaller chord lengths toward the tip, also requiring a re-arrangement of the twist law, and a redistribution of the leading edge sweep angles along a wider range of the blade span. This new planform shape was therefore characterised by a smaller solidity which increased the blade loading;

2. the simple rotor speed reduction was beneficial both in terms of total power reduction and noise abatement for all the flight conditions investigated. Nevertheless, the planform optimization contributed at improving these benefits;
3. the combined effects of rotor speed reduction and planform optimization produced power reductions ranging from 3.52%, in hover flight, to 5.96%, in fly-over flight, and noise reductions ranging from 1.88dB, in fly-over flight, to 3.40dB, in descent flight;
4. the optimization procedure turned out to be not beneficial for the power reduction in descent flight and the noise reduction in cruise fight. However, this outcome was deemed not crucial for the performance improvement of the rotor standing the little contribution of each of the two flight conditions to the respective design objectives.

Future activities will be addressed at analysing in more detail the performance of the baseline and the optimized rotors by using more sophisticated aeromechanic and aeroacoustic tools in order to confirm the validity of the results obtained by the present optimization procedure.

11 ACKNOWLEDGMENTS

This research activity was funded by the Clean Sky Joint Undertaking under projects GAM-GRC, related to activities performed within the ITD Green Rotorcraft.

12 REFERENCES

[1] Prouty, R.W., “Should We Consider Variable Rotor Speeds?,” Vertiflite, A Publication of the American Helicopter Society, Vol. 50, No. 4, 2004;

[2] Kang, H., Saberi, H., Gandhi, F., “Dynamic Blade Shape for Improved Helicopter Rotor Performance,” Journal of the American Helicopter Society, Vol.55, Nr.3, July 2010;

[3] Antifora, A., Toulmay, F., “Clean Sky - The Green Rotorcraft Integrated Technology Demonstrator - State of Play Three Years After Kick-Off, 37th European Rotorcraft Forum, Ticino Park, Italy, Sep. 13th – 15th, 2011;

[4] http://www.noesissolutions.com/Noesis/ ;

[5] Advanced Rotorcraft Technology, Inc, “FLIGHTLAB Software,” www.flightlab.com;

[6] He, C. J., Lee, C.S., and Chen, W., “Rotorcraft simulation model enhancement to support design, testing and operational analysis,” Journal of the American Helicopter Society, Vol.45, No. 4, pp. 284-292, Oct. 2000;

[7] Du Val, R.W., "A Real-Time Multi-Body Dynamics Architecture for Rotorcraft Simulation," Royal Aeronautical Society and American Helicopter Society International Conference on The Challenge of Realistic Rotorcraft Simulation, London, UK, 7-8 Nov. 2001;

[8] Peters, D.A., He, C.J., “Finite State Induced Flow Models Part II: Three-Dimensional Rotor Disk,” Journal of Aircraft, Vol. 32, No. 2, pp 323-332, Mar.-Apr. 1995;

[9] Peters, D.A., He, C. J., “Correlation of Measured Induced Velocities with a Finite-State Wake Model,” American Helicopter Society 45th Annual Forum, Boston, May 1989;

[10] Advanced Rotorcraft Technology, Inc, “FLIGHTLAB Theory Manual (Vol. Two),” July 2011;

[11] Bhagwat, M.J., Leishman, J.G., “Generalized Viscous Vortex Model for Application to Free-Vortex Wake and Aeroacoustics Calculations,” American Helicopter Society 58th Annual Forum Proceedings, Montreal, June 11-13 2002;

[12] Bhagwat, M.J., Leishman, J. G., “On the Stability of Helicopter Rotor Wakes,” American Helicopter Society 56th Annual Forum Proceedings, Virginia Beach, May 2-4 2000;

[13] Kufeld, R.M., Balough, D.L., Cross, J.L., Studebaker, K.F., Jennison, C. D., and Bousman, W.G., “Flight Testing of the UH-60A Airloads Aircraft,” American Helicopter Society 50th Annual Forum Proceedings, Washington, D.C., May 1994;

[14] Yeo, H., Bousman, W.G., Johnson, W., “Performance Analysis of a Utility Helicopter with Standard and Advanced Rotors,” Journal of the American Helicopter Society, Vol. 49, N.3, July 2004;

[15] Casalino, D., “An Advanced Time Approach for Acoustic Analogy Predictions,” Journal of Sound and Vibration, Vol. 261, No. 4, 2003, pp. 583–612;

[16] Casalino, D., Barbarino, M., Visingardi, A., “Simulation of Helicopter Community Noise in Complex Urban Geometry”, AIAA Journal, Vol. 49, No. 8, 2011, pp. 1614-1624;

[17] Langer, H.-J., Dieterich, O., Oerlemans, S., Schneider, O., van der Wall, B., Yin, J., “The EU HeliNOVI Project - Wind Tunnel Investigations for Noise and Vibration Reduction,” presented at the 31st European Rotorcraft Forum, Florence (I), 13-15 Sept. 2005;

[18] Leishman, J.G., “Principles of Helicopter Aerodynamics,” Eds. Rycroft, M.J., Stengel, R.F.,Cambridge University Press, 2000;

[19] Yin, J., Dummel, A., Falchero D., Pidd, M., Prospathopoulos, J., Visingardi, A., Voutsinas, S.G., “Analysis of Tail Rotor Noise reduction Benefits Using HeliNOVI Aeroacoustic Main/Tail Rotor Test and Post-Test Prediction Results,” presented at the 32nd European Rotorcraft Forum, Maastricht (NL), 12-14 Sept. 2006.

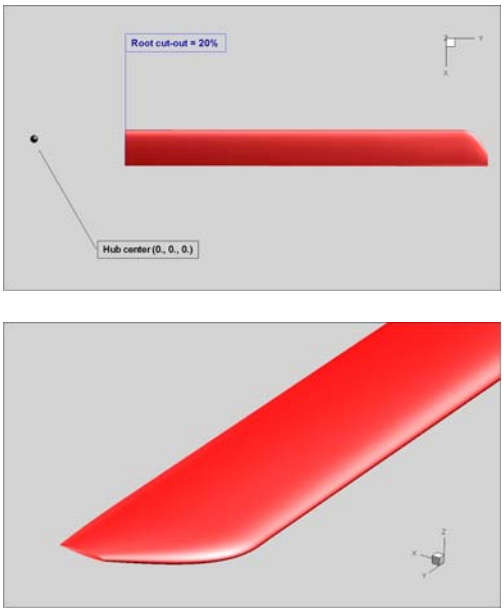

Figure 1: Baseline blade planform (top) and tip detail (bottom)

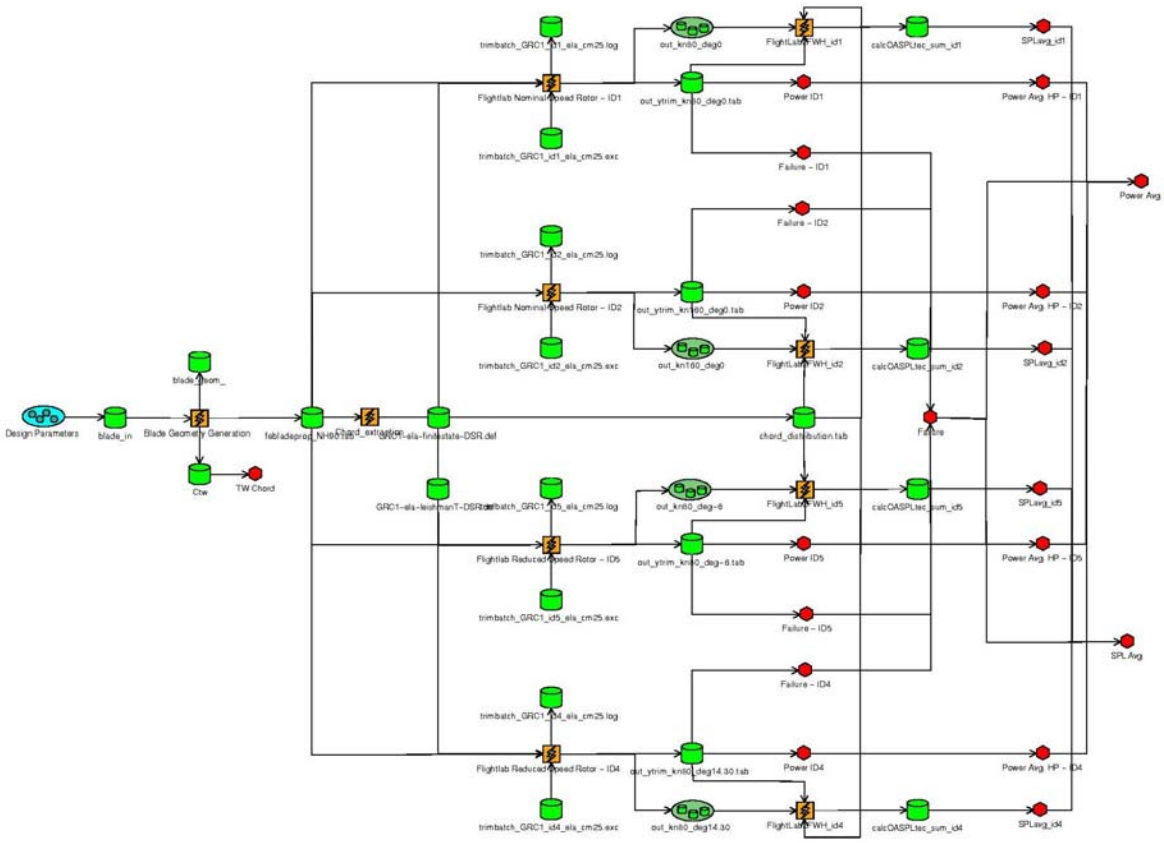

Figure 2: Workflow of the optimization procedure

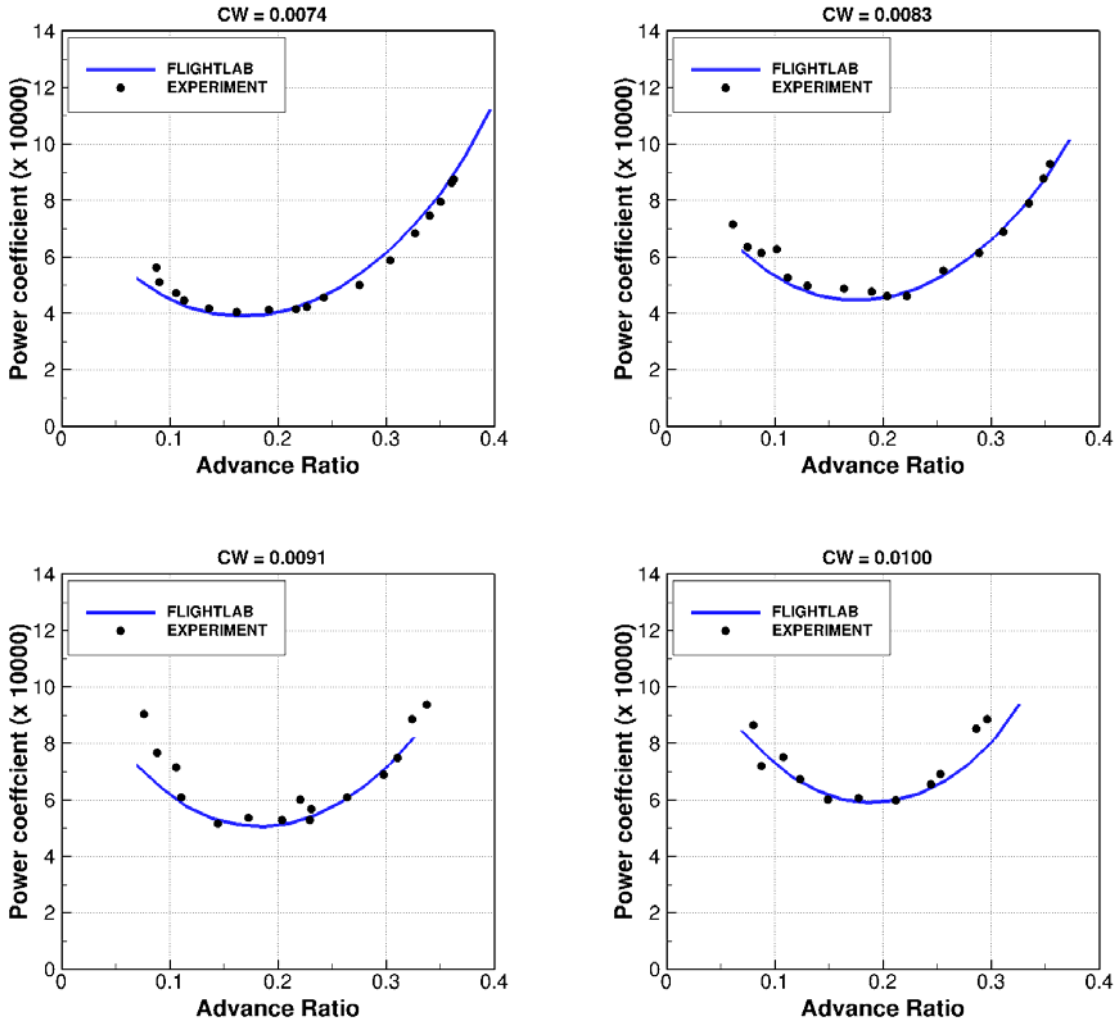

Figure 3: FlightLab power predictions vs experimental data

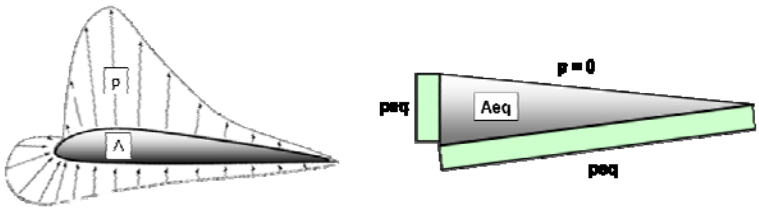

Figure 4: FRN model concept: a) chordwise pressure distribution (left); b) equivalent pressure distribution (right)

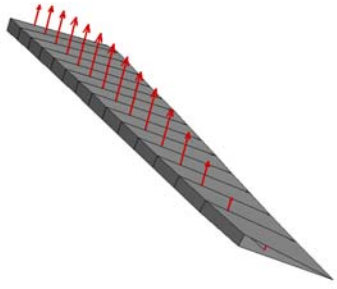

Figure 5: FRN equivalent blade

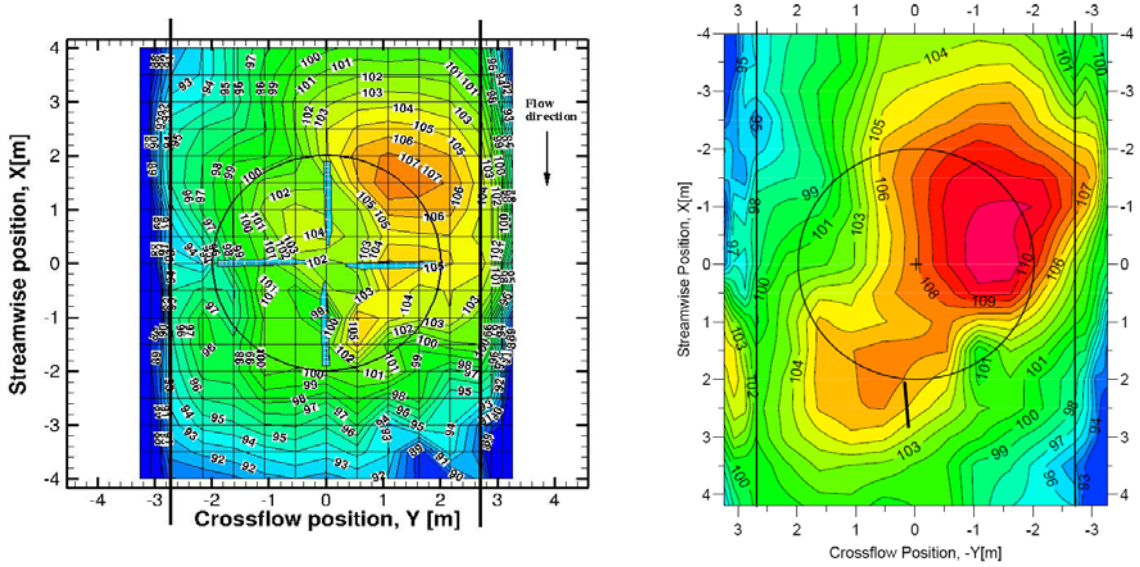

Figure 6: Noise Carpets: FRN estimation (left), measured (right) – 6° Descent flight

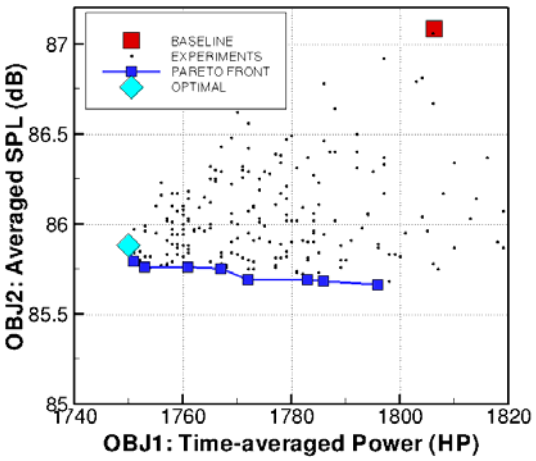

Figure 7: Evaluation of the optimal solution

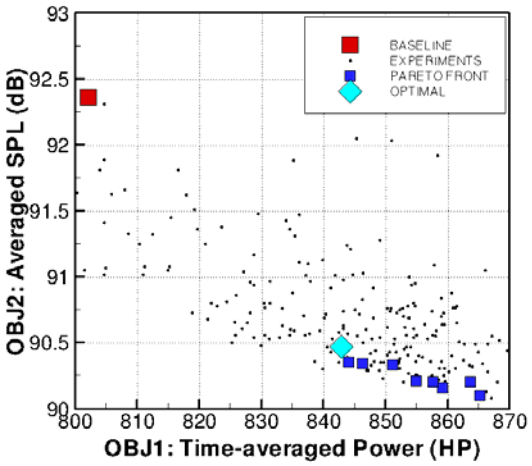

Figure 8: Evaluation of the optimal solution in 80 kts 6° descent flight

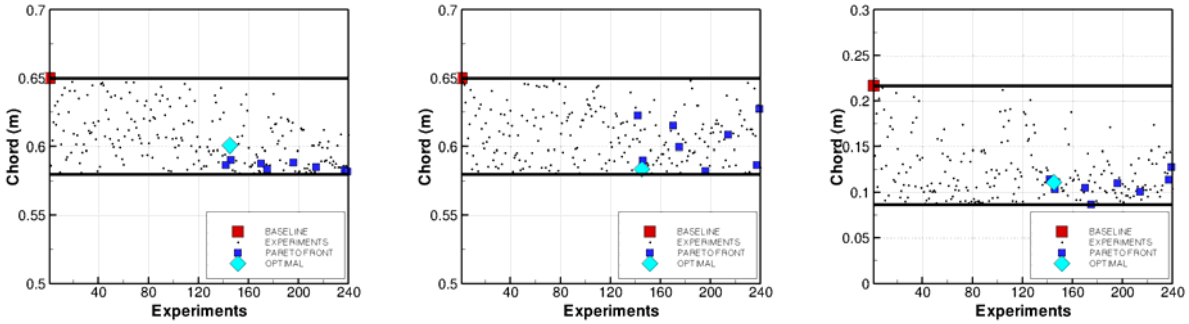

a) Chord length evolution: r/R = 75% (left); r/R = 95% (centre); r/R = 100% (right)

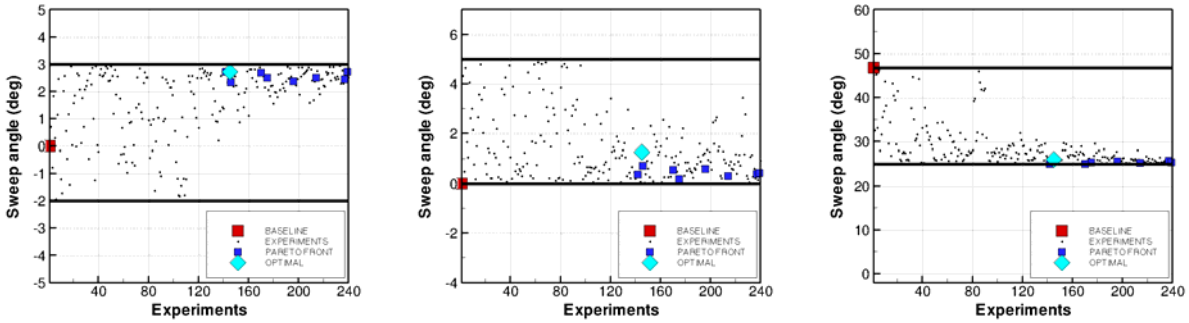

b) Sweep angle evolution: r/R = 47% (left); r/R = 75% (centre); r/R = 95% (right)

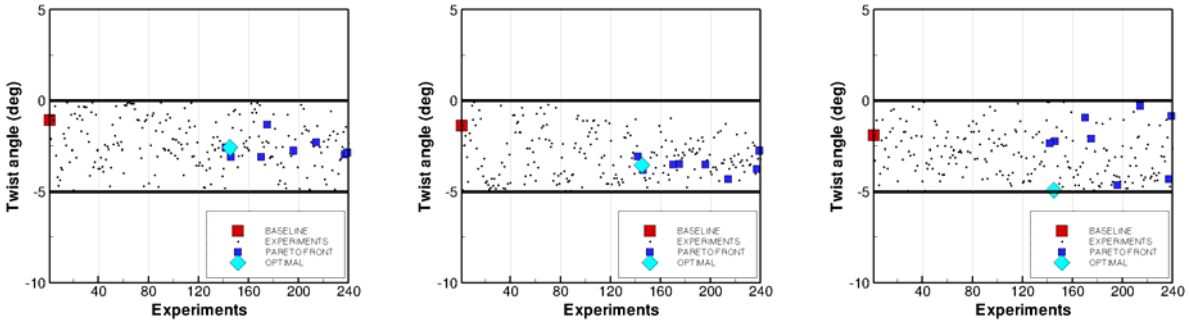

c) Twist angle evolution: r/R = 75% (left); r/R = 95% (centre); r/R = 100% (right)

Figure 9: The evolution of the design parameters during the optimization procedure

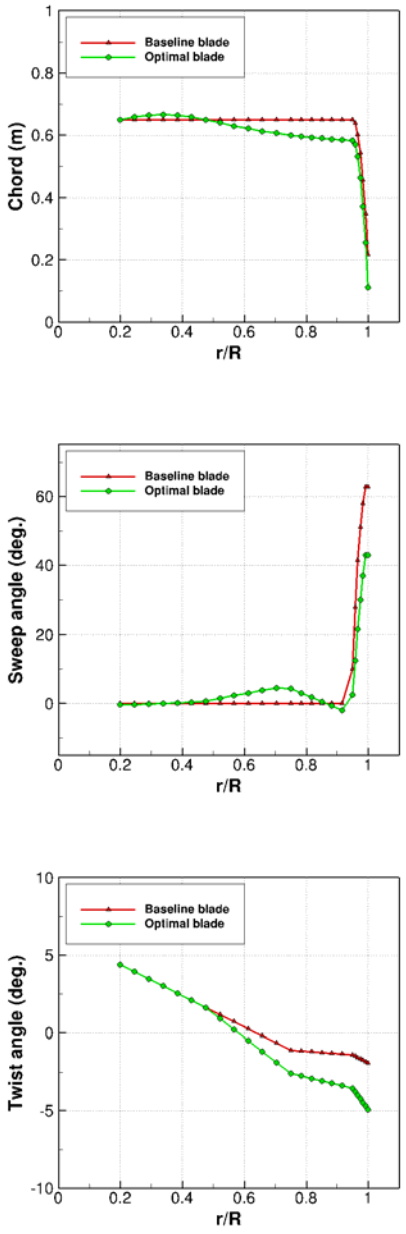

Figure 10: Chord (top), sweep (centre) and twist (bottom) distributions

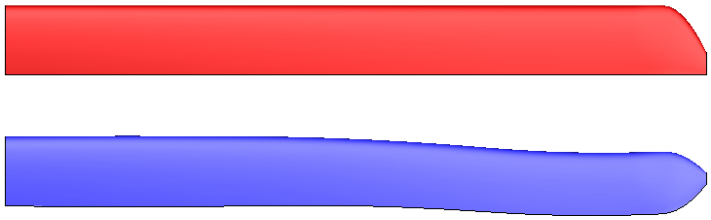

Figure 11: Baseline (top) and Optimized (bottom) blade planforms

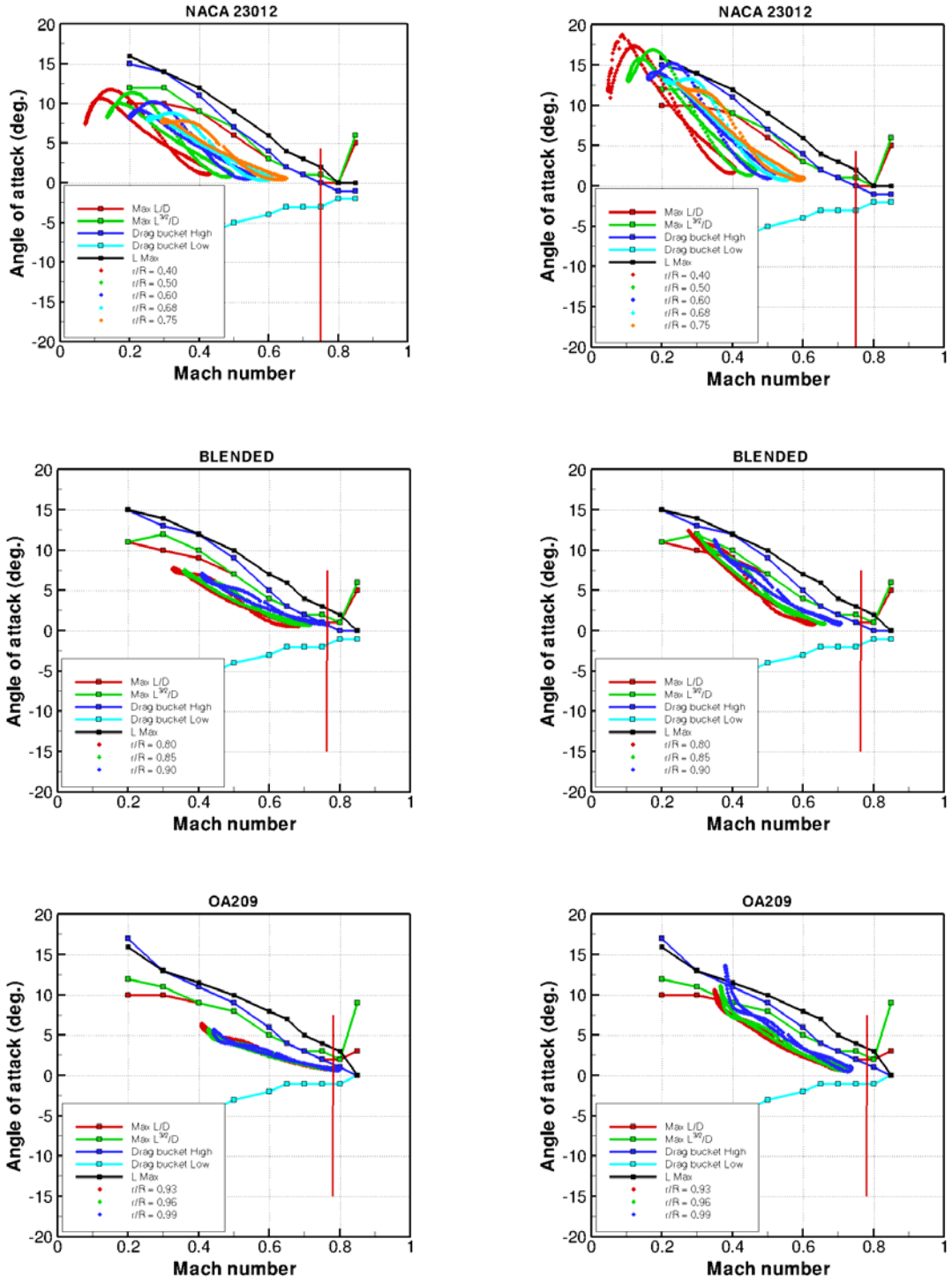

Figure 12: Angle of attack vs Mach number for the fly-over 120 kts level flight. Baseline blade airfoil sections @ 100%RPM (left); optimized blade airfoil sections @ 90%RPM (right)

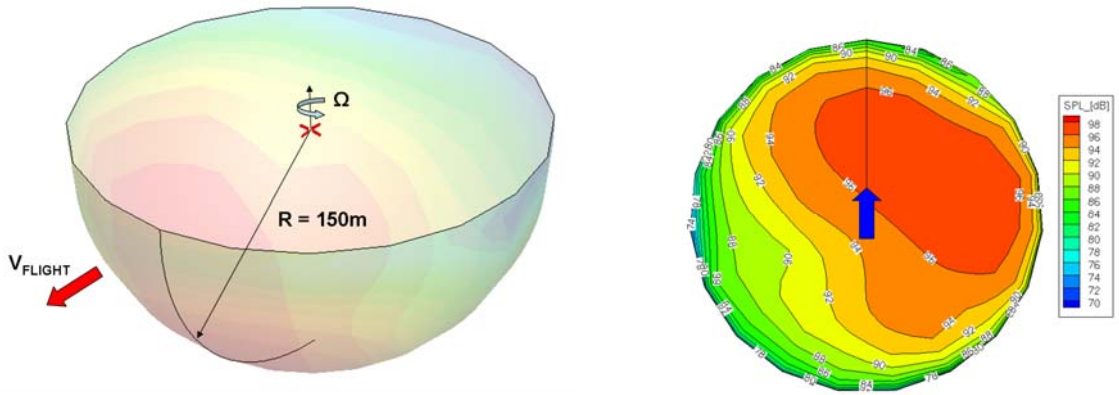

a) Hemisphere of microphones for OASPL evaluation

b) Baseline rotor @ 100%RPM

b) Baseline rotor @ 90%RPM

b) Optimized rotor @ 90%RPM

Figure 13: OASPL distributions on a hemisphere –6° Descent flight 80 kts.

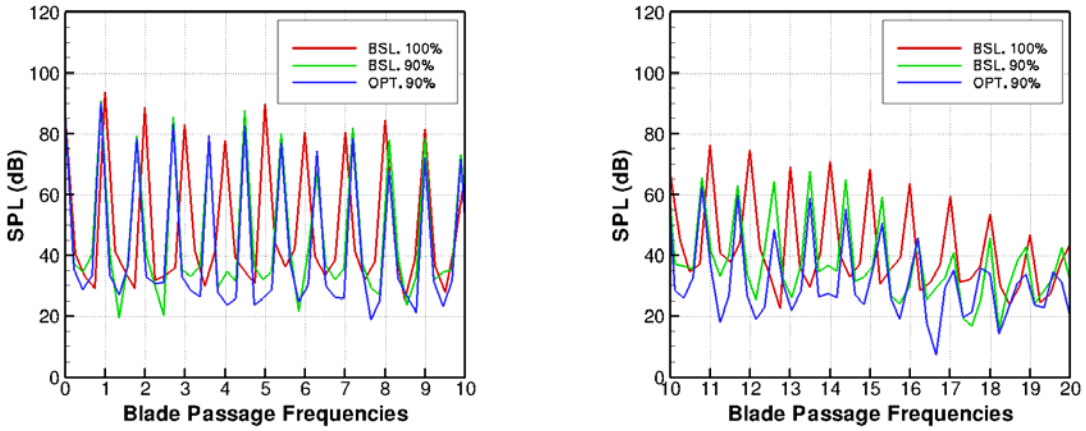

Figure 14: Noise spectra vs blade passage frequency – 6° Descent flight 80 kts.